2009-01-0403

Modeling a Slider-Crank Mechanism With Joint Wear

Saad Mukras, Nathan A. Mauntler, Nam H. Kim, Tony L. Schmitz and W. Gregory Sawyer
University of Florida

ABSTRACT

The paper presents a study on the prediction of wear for systems in which progressive wear affects the operating conditions responsible for the wear. A simple slider-crank mechanism with wear occurring at one of the joints is used to facilitate the study. For the mentioned mechanism, the joint reaction force responsible for the wear is, itself, affected by the progression of wear. It is postulated that the system dynamics and the wear are coupled and evolved simultaneously.

The study involves integrating a dynamic model of the slider-crank mechanism (with an imperfect joint) into a wear prediction procedure. The prediction procedure builds upon a widely used iterative wear scheme. The accuracy of the predictions is validated using results from an actual slider-crank mechanism.

INTRODUCTION

Clearances at the joints of multibody systems (usually due to manufacturing tolerance) have been noted to affect the performance and service life of mechanical systems. This may be attributed to the increased vibration, excessive wear and dynamic force amplification as discussed by Dubowsky [1]. Due to the significance of the problem, numerous studies have been conducted with the goal of understanding the dynamic response of these systems in the presence of joint clearances [1-16]. These studies have evolve from the analysis of less complex planar multibody systems [1-3, 5-11, 13,14,16] to more complex spatial systems [4, 15] as well as from rigid multibody analysis [1,2,5-10,12-16] to flexible multibody analysis [3,4,11]. The studies have demonstrated that the presence of clearances alter the response of the system appreciably.

Although these studies will go a long way into allowing designers to take into account joint clearance, the findings may be limited to the idealized case in which wear is assumed to be nonexistent. This is contrary to a realistic scenario in which wear is expected to increase the clearance size and thus further alter the system response. This research seeks to address this issue by allowing the joint clearance to vary as dictated by the wear. As a result, the system dynamics will evolves with the wear and this evolution is captured by an integrated model presented in the article. The effect of the wear on the system dynamics and conversely the effect of the evolving dynamics on the wear can then be studied.

In the first part of the paper a wear prediction procedure is presented. The procedure presented is based on a widely used finite-element-based iterative wear prediction procedure. In the next part, modeling of a perfect and imperfect joint is discussed. Two different kinds of imperfect joints are discussed. The first being a general imperfect joint model in which the two components of the joint are allowed to move relative to each other depending on the dynamic behavior of the system. The second model is a simplified and more specific case to the study (slider-crank mechanism), in which the two components of the joint are in continuous contact. Next, the wear prediction procedure is integrated with the model that describes the imperfect joint. Only the simplified joint case is considered for the integration. In the final part of the report, the experimental validation of the integrated model is discussed.

WEAR PREDICTION

In the case of a revolute joint of a mechanical system, wear would occur when the components of the joint are in contact and in relative motion. The amount of wear at such a joint is affected by the type of material the components are made of, the relative sliding distance and the operating conditions. Here, the operating conditions refers to the amount of reaction force developed at the joint and the condition of the joint which could be dry, lubricated, or contaminated with impurities.

A lot of effort has been placed in developing models to predict wear occurring in components similar to those of the revolute joint. Majority of these models are based on the Archard's wear law, first published by Holm [17] in 1946. One form of the equation is express mathematically as follows:

$$\frac{hA}{s} = kF_N, \tag{1}$$

where s is the sliding distance, k is a wear coefficient, h is the wear depth, A is the contact area and F_N the applied normal force. Equation (1) can further be simplified by noting that the contact pressure may be expressed with the relation $p = F_N / A$ so that the wear model is expressed as

$$\frac{h}{s} = kp \, . \tag{2}$$

The wear process is generally considered to be a dynamic process (rate of change of the wear depth with respect to the sliding distance) so that the differential form of Eq. (2) can be expressed as

$$\frac{dh}{ds} = kp(s) \, , \tag{3}$$

where the sliding distance is considered as a time in the dynamic process. A numerical solution for the wear depth may be obtained by estimating the differential form in Eq. (3)with a finite divide difference to yield the following updating formula for the wear depth:

$$h_i = h_{i-1} + kp_i \Delta s_i \, . \tag{4}$$

In Eq.(4), h_i refers to the wear depth at the i^{th} cycle while h_{i-1} represents the wear depth at the previous cycle. The last term in Eq. (4) is the incremental wear depth which is a function of the contact pressure (p_i) and the incremental sliding distance (Δs_i) at the corresponding cycle. Thus if the wear coefficient, the contact pressure and the incremental sliding distance are available at every cycle, the overall wear can be estimated. To that end, the value of the wear coefficient can be obtained through experiments as discussed in the literature,[22, 24-26] where as the contact pressure can be calculated using Finite element analysis (FEA) or the Winkler Surface model [22]. Since the Finite element method is more superior than the FEA, with regard to accuracy, only the FEA method is adopted in this reserach. The incremental sliding distance can be obtained as a result of the FEA or may be specified explicitly. In this work the commercial finite element program ANSYS has been employed in conjunction with the corresponding design language, Ansys Parametric Design language (APDL).

A number of papers [18-24] which demonstrate the implementation of Eq. (4) in estimating wear have been published. Although the details of the various procedures differ, three main steps are common to all of them. These include the following:

- Computation of the contact pressure resulting from the contact of bodies.
- Calculation of the incremental wear amount based on the wear model.
- Geometry update by moving the contact boundary to reflect the wear and to provide the new geometry for the next cycle (this allows for a more accurate and realistic prediction of the wear process).

The wear prediction procedure employed in this research incorporates the three steps mentioned. It should, however, be mentioned that the wear simulation procedure is a computationally expensive process. This is due to the number of cycles that need to be simulated (usually greater than 10,000 cycles) each of which requiring some type of analysis to determine the contact pressure and sliding distance. In order to mitigate the computational costs, an extrapolation procedure was used. This involves calculating the incremental wear depth for a representative cycle and then extrapolating this wear depth over N fixed cycles. The use of an extrapolation results in a modification of the updating formula (4). The new equation is expressed as:

$$h_i = h_{i-1} + kA_E p_i \Delta s_i \, , \tag{5}$$

where A_E is the extrapolation factor. The choice of the extrapolation is critical to the efficiency and stability of the simulation. The use of large extrapolations will cause the simulation to be unstable and compromise the accuracy of the simulation. On the other hand using small extrapolation sizes will result in a less than optimum use of resources. A complete study on extrapolations, its effect on stability of wear prediction and optimizing its selection can be found in our previous work [24].

A flowchart summarizing the simulation procedure is shown in Fig.1. The procedure will later be integrated with the dynamic model for the imperfect slider-crank mechanism, which is discussed in the next section.

MODELING IMPERFECT REVOLUTE JOINTS

Revolute joints in mechanical systems are generally imperfect. This means that the joints have some amount of clearances usually due to constraints and requirements in manufacturing. In addition, throughout the service life of the system the clearances increase in size due to wear. As was mentioned earlier, the clearance affects the dynamics of system. In this section two imperfect joint models that have the capability of accounting for changes in system dynamics due to clearances size changes are discussed.

To facilitate the study, a slider-crank mechanism has been used, due to its simplicity. A diagram of the slider-crank mechanism to be used in the study is shown in Fig. 2. The study is simplified by eliminating friction and wear from all connection points in the mechanisms except for one joint, shown as the joint of interest in Fig. 2. This joint essentially consists of a pin that is attached

to the crank (drive-link Fig. 2.) and a bushing attached to the connecting rod (driven-link). The pin is made of hardened steel and is assumed to be hard enough so that no appreciable wear occurs on its surface. The bushing on the other hand is made of poly-tetra-fluoro-ethene (PTFE) which is soft and will experience considerable wear. A spring is attached to the slider which serves as a means to increase the joint reaction force and hence accelerated the wear occurring at the joint.

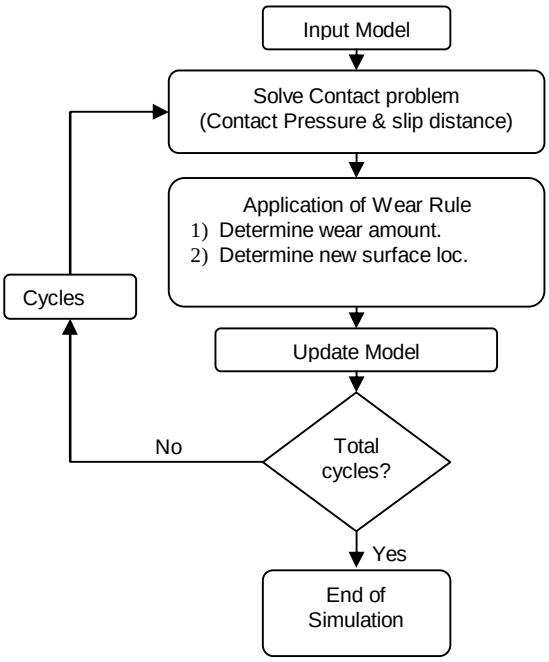

Figure 1: Wear simulation flow chart.

In order to successfully study the dynamic response of the mechanism under joint wear, it is necessary to develop a formulation for the slider-crank system that estimates the changes to the system dynamics when the joint clearance is changed. In what follows, a formulation for the dynamic and kinematic analysis of the slider-crank mechanism with perfect joints is presented. Based on this formulation, the model for the slider-crank mechanism with an imperfect joint will be developed.

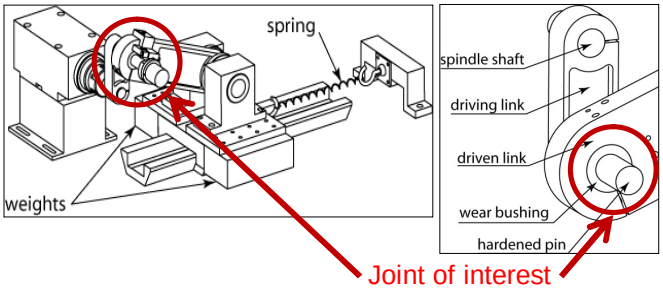

Figure 2: Slider-crank mechanisms to be used in the wear study.

DYNAMICS OF A SLIDER-CRANK MECHANISM WITH PERFECT JOINTS - In a slider-crank mechanism with perfect joint, the pin is assumed to fit perfectly in the bushing. Consequently the pin and bushing centers coincide at all times. The slider-crank system is assumed to consist of three rigid bodies with planar motion as depicted in Fig. 3. The three disassembled components of the mechanism (link-1, link-2 and a slider) are shown in the global axis. Each component can translate and rotate in the plane.

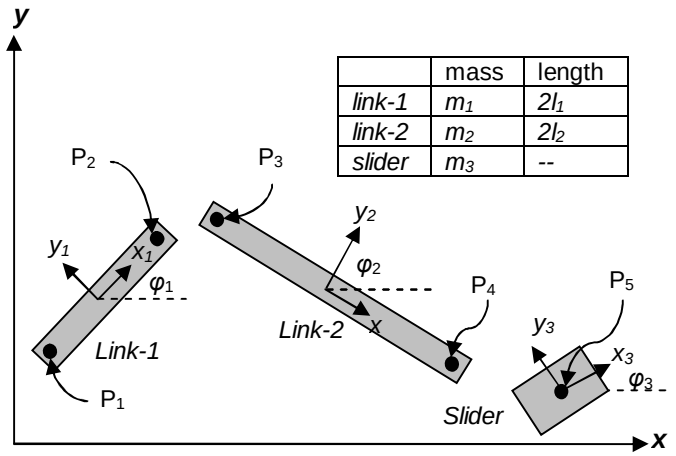

	mass	length
link-1	m_1	$2l_1$
link-2	m_2	$2l_2$
slider	m_3	--

Figure 3: Components of the slide crank mechanisms.

The kinematics of the system is determined by imposing constraints on the motion of the components. The constraints corresponding to the slider-crank mechanism shown in Fig. 3. consist of nine nonlinear simultaneous equations expressed as:

$$\mathbf{\Phi} = \begin{bmatrix} x_1 - l_1\cos\phi_1 \\ y_1 - l_1\sin\phi_1 \\ x_2 - 2l_1\cos\phi_1 - l_2\cos\phi_2 \\ y_2 - 2l_1\sin\phi_1 - l_2\sin\phi_2 \\ x_3 - 2l_1\cos\phi_1 - 2l_2\cos\phi_2 \\ y_3 - 2l_1\sin\phi_1 - 2l_2\sin\phi_2 \\ y_3 \\ \phi_3 \\ \phi_1 - \omega t \end{bmatrix} = \begin{bmatrix} 0 \\ 0 \\ 0 \\ 0 \\ 0 \\ 0 \\ 0 \\ 0 \\ 0 \end{bmatrix} \quad (6)$$

The first two constraints in Eq. (6) confine point P1 on link-1 to the origin. The next two constraints ensure that points P2 on link-1 and P3 link-2 coincide at all times. This condition is synonymous to a perfect joint and later will be relaxed when modeling the imperfect joint. The fifth and sixth constrains in Eq. (6) represent the perfect revolute joint between Link-2 and the slider. The next two constraints ensures that the slider remain on the x-axis without rotation. The final constraint, known as the driving constraint, is an external input such as a servo motor that specifies the motion of one of the links. For the current case a constant angular velocity ω is imposed in link-1.

It can be seen from the set of simultaneous equations above, that the number of equations exactly equals the number of unknowns. The unknowns are the DOFs of

the components at the center of masses. This is denoted by vector q, as

$$\mathbf{q} = \left[x_1, y_1, \phi_1, x_2, y_2, \phi_2, x_3, y_3, \phi_3\right]^T . \quad (7)$$

The set of simultaneous nonlinear equations (Eq. (6)) can be solved simultaneously to determine the slider-crank mechanism component positions at any instant. The velocities and accelerations may also be determined using the following relations:

$$\dot{\mathbf{q}} = -\boldsymbol{\Phi}_{\mathbf{q}}^{-1}\boldsymbol{\Phi}_t \quad (8)$$

$$\ddot{\mathbf{q}} = \boldsymbol{\Phi}_{\mathbf{q}}^{-1}\left(-\left(\boldsymbol{\Phi}_{\mathbf{q}}\dot{\mathbf{q}}\right)_{\mathbf{q}}\dot{\mathbf{q}} - 2\boldsymbol{\Phi}_{\mathbf{q}t}\dot{\mathbf{q}} - \boldsymbol{\Phi}_{tt}\right) \quad (9)$$

Once the accelerations have been computed, the reaction forces can be obtained through the process of reverse dynamics. However, if we desire to obtain the response of the system due to externally applied forces, such as a spring force (see Fig. 2.) or a torque applied instead of the drive constraint, then a dynamic analysis is required. This involves assembling and solving the differential-algebraic equations of motion (DAE). This equation is expressed as follows;

$$\begin{bmatrix} \mathbf{M} & \boldsymbol{\Phi}_{\mathbf{q}}^{\mathbf{T}} \\ \boldsymbol{\Phi}_{\mathbf{q}} & \mathbf{0} \end{bmatrix}\begin{bmatrix} \ddot{\mathbf{q}} \\ \boldsymbol{\lambda} \end{bmatrix} = \begin{bmatrix} \mathbf{Q}_{\mathbf{A}} \\ \boldsymbol{\Phi}_{\mathbf{q}}\ddot{\mathbf{q}} \end{bmatrix}, \quad (10)$$

where $\mathbf{M}$ is a diagonal mass matrix, $\boldsymbol{\Phi}_{\mathbf{q}}$ is the Jacobian of the constraint vector, $\ddot{\mathbf{q}}$ is the acceleration vector, $\boldsymbol{\lambda}$ is a vector of Lagrange multipliers and $\mathbf{Q}_{\mathbf{A}}$ is the vector of externally applied forces. The solution procedure for this equation, to obtain the dynamics of a system, is well documented in the literature [14, 28,29]. An summary of the solution procedure is shown in Fig. 4.

DYNAMICS OF A SLIDER-CRANK MECHANISM WITH AN IMPERFECT JOINT - Two kinds of the imperfect joints for the slider-crank mechanism, a general imperfect joint and a simplified imperfect joint are discussed. The first imperfect joint can be found in the literature [13,14,16] and is only briefly discussed. It is used as a reference for comparison with the simplified imperfect joint.

Modeling a General Imperfect Joint - The general imperfect joint consists of two components (pin and bushing) that are allowed to move relative to each other depending on the dynamics of the system. A slider-crank mechanism with an imperfect joint is illustrated in Fig. 5.

For this joint, the condition previously used in the perfect joint formulation that required the pin and bushing centers to coincide ceases to be valid. The slider-crank mechanism in this case is thus modeled by eliminating the two constraints so that the new kinematic constrain in Eq. (6) reduces to the expression shown in Eq. (11). The imperfect joint can then be realized by ensuring that the motion of the pin is confined within the inner perimeter of the bushing. This can be achieved by imposing a force constraint on both components whenever they establish contact as discussed by Flores [15].

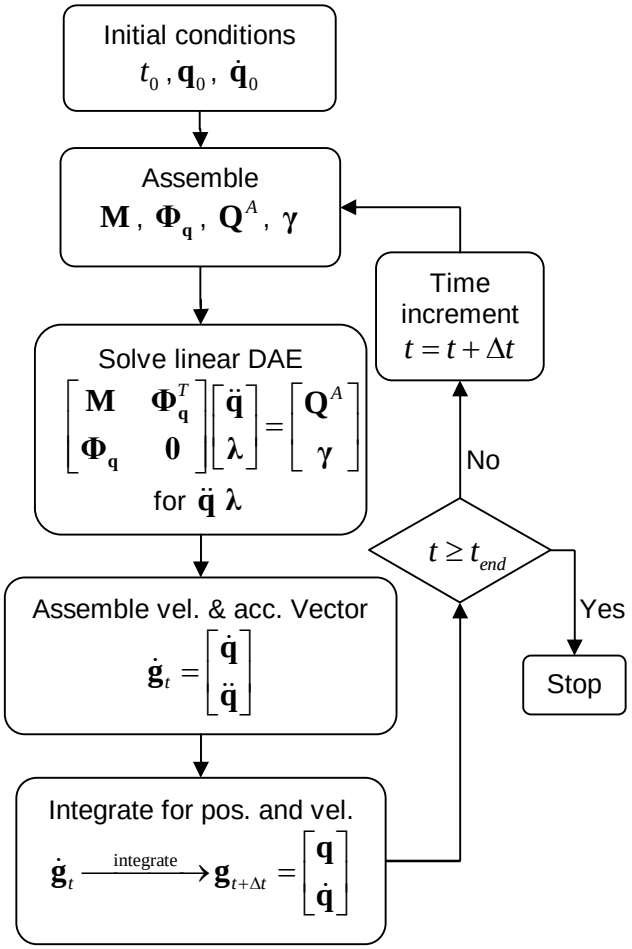

Figure 4: Solution procedure for the Differential Algebraic Equation.

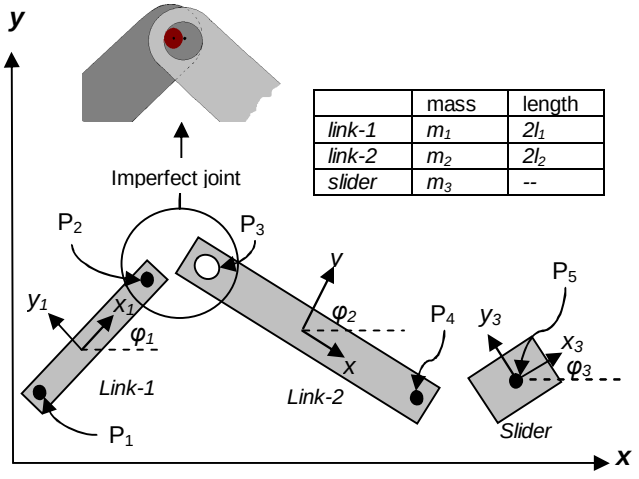

Figure 5: Disassembled slider-crank mechanisms with an imperfect joint.

$$\mathbf{\Phi} = \begin{bmatrix} x_1 - l_1\cos\phi_1 \\ y_1 - l_1\sin\phi_1 \\ x_2 - x_3 + l_2\cos\phi_2 \\ y_2 - y_3 - l_2\sin\phi_2 \\ y_3 \\ \phi_3 \\ \phi_1 - \omega t \end{bmatrix} = \begin{bmatrix} 0 \\ 0 \\ 0 \\ 0 \\ 0 \\ 0 \\ 0 \end{bmatrix}. \quad (11)$$

The force constraint is essentially the reaction force developed upon contact. It is assumed that the region where the contact is established is deformable so that the reaction force can be estimated by a contact force law. A contact force model with hysteresis damping, discussed by Hamid [30], can be employed. The model is expressed as follows:

$$F_N = K\delta^{1.5}\left(1 + \frac{3\left(1-e_r^2\right)}{4}\frac{\dot{\delta}}{\dot{\delta}^{(-)}}\right) \quad (12)$$

where F_N is the reaction force, δ is the penetration between the pin and bushing, e_r is the coefficient of restitution, $\dot{\delta}$ is the penetration velocity, $\dot{\delta}^{(-)}$ is the initial penetration velocity upon impact and K is a constant that is dependent on the material properties of the components and their geometry. The constant is expresses as follows,

$$K = \frac{4}{3\left(h_i + h_j\right)}\left(\frac{R_i R_j}{R_i + R_j}\right)^{\frac{1}{2}}$$
$$h_n = \frac{1-\upsilon_n^2}{E_n} \qquad n = 1,2 \quad (13)$$

where R_n is the radius of the pin and bushing, υ_n is the Poisson ratio of the components and E_n is the elastic modulus of the components.

In addition to the reaction forces, the friction force can be determined by using the Coulomb friction model shown in the following equation:

$$F_f = \mu F_N, \quad (14)$$

where μ is the coefficient of friction and F_N is the normal force as previously described.

For the general imperfect joint a kinematic analysis cannot be performed since the jacobian of the constraint vector (Eq. (11)) is not square. A dynamic analysis is necessary. The differential-algebraic equation of motion can be assembled as described in the previous section (Eq. (10)). Both the contact and friction forces are included in the applied force vector $\mathbf{Q}_A$ of Eq. (10). The dynamics of the system can then be obtained by solving the assembled DAE.

The general imperfect joint model that has been discussed allows the system dynamics of the slider-crank mechanisms with an imperfect joint to be determined. This is done by specifying the radius of the pin and bushing to reflect the joint clearance. As an example, the dynamics of the system with parameters shown in Table 1 and Table 2 is determined. A value of 0.8 was used for the coefficient of restitution where as no friction was considered. Figure 6a. illustrates the effect of different clearance sizes on the joint reaction force for this system as a function of the crank position (in radians). In the figure, the second crank cycle is plotted. As was expected, dynamics of the system is altered when the joint clearance size is varied. When the pin and bushing radius are approximately equal the imperfect and the perfect joint models should yield identical results. Figure 6b shows the comparison of the reaction force from the perfect and imperfect joint models when the clearance is approximately zero.

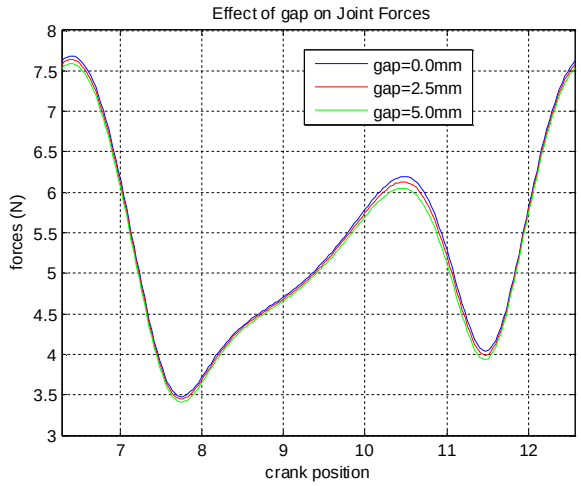

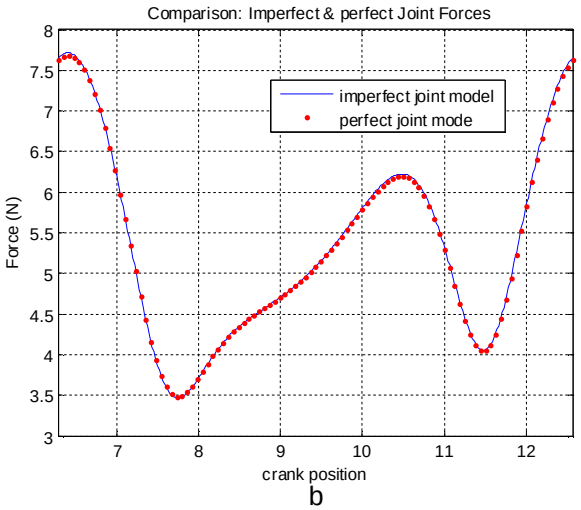

Figure 6: a) Reaction force plot for various clearance sizes. b) Reaction force for the perfect and general imperfect joint models (zero clearance).

Table 1: Dimension and mass properties of the slide-crank mechanism.

	Length (m)	Mass (kg)	Inertia x10^{-6} (kg.m^2)
Link 1	0.0381	0.4045	204.0
Link 2	0.1016	0.8175	5500.0
Slider	-	5.5487	-

Table 2: Properties of the pin and bushing

	Pin	Bushing
Initial radius	9.525 mm	9.535 mm
Poisson ratio	0.29	0.38
Young's Modulus	206.8 MPa	0.139 MPa

Modeling a Simplified Imperfect Joint - In the previous section a general imperfect joint model was presented. In this section a simplified joint model is presented. The simplified model does not assume local deformation at the location of contact consequently no contact force model is required. As a result it is computationally cheaper than the previous model. The model is, however, specific to this application (as will be outlined in the assumption) but can be modified to suit other applications.

The diagram of a slider-crank mechanism with an imperfect joint was shown in Fig. 5. This mechanism is identical to the slider-crank mechanism with perfect joint except for the imperfect joint. As a result the constraints equations for both slider-crank mechanisms are similar except for the imperfect joint. This was also true for the case of the general imperfect joint. We shall therefore focus our attention on formulating the imperfect joint as we did in the previous case.

In modeling the simplified imperfect joint three assumptions are made. These assumptions are as follows:

1. It is assumed that the pin will be in contact with the bushing at all the times.

2. It is also assumed that the region on the bushing where the pin first establishes contact with the bushing does not change. The center point of this region is shown as point *C* in Fig 7.

3. Final it is assumed that the pin center, the bushing center, and the contact point *C* will remain collinear at all times.

With these assumptions in place, the constraint equations relating to the imperfect joint can be derived with the aid of Fig.7. It is noted that an additional variable (α), not encountered in the previous formulations, is required in deriving the imperfect joint constraint. The addition variable (α) describes the angle between the local *x*-axes of the two links. It also allows for the determination of the center point of contact region of the pin at any instant of the motion. This information will be required when determining the relative sliding distance between the pin and the bushing.

The imperfect joint constraints are formulated by imposing two conditions. These are described as below:

1. Since the pin and bushing are assumed to be in contact at all times, a loop starting from the origin to the center point of contact (point *C*) and back to the origin should be closed. In Fig. 7., this loop is described by vectors that follow the path *O-A-B-C-D-E-O*. This loop can be represented mathematically as follows:

$$\mathbf{r}_1 + \mathbf{A}_1\mathbf{s}_1 + \mathbf{A}_{11}\mathbf{a}_1 - \mathbf{A}_2\mathbf{s}_2 - \mathbf{A}_2\mathbf{a}_2 - \mathbf{r}_2 = \mathbf{0} \qquad (15)$$

where $\mathbf{A}_1$, $\mathbf{A}_{11}$ and $\mathbf{A}_2$ are transformation matrices that transform the local vector $\mathbf{s}_1$, $\mathbf{a}_1$ and $\mathbf{s}_2$, and $\mathbf{a}_2$ into global vectors, respectively. This yields two constraint equations that can be written as follows:

$$\begin{bmatrix} -x_2 + 2l_1\cos\phi_1 + R_1\cos(\phi_1+\alpha) + [R_2+l_2]\cos\phi_2 \\ -y_2 + 2l_1\sin\phi_1 + R_1\sin(\phi_1+\alpha) + [R_2+l_2]\sin\phi_2 \end{bmatrix} = \begin{bmatrix} 0 \\ 0 \end{bmatrix} \qquad (16)$$

where R_1 and R_2 are the radius of the pin and bushing respectively.

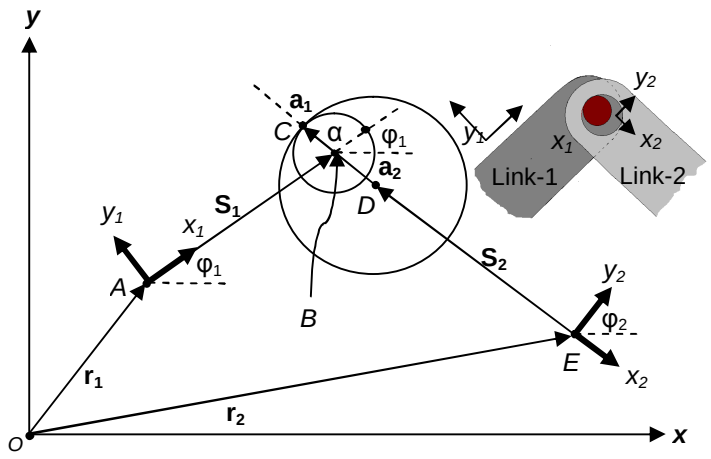

Figure 7: Variable defining the simplified imperfect joint.

2. The second constraint requires that the vector along the line *B-C* and the vector along *D-C*, to be parallel. The vector along line *B-C*, expressed as $\mathbf{g}_1 = \mathbf{A}_{11}\mathbf{a}_1$, is the vector that runs from the center of the pin to the point of contact. It is noted that this vector, in both local and global coordinated systems, changes its orientation according to the variable α when the mechanism is in motion. On the other hand, the vector along line *D-C*, expressed as $\mathbf{g}_2 = \mathbf{A}_2\mathbf{a}_2$, does not change its orientation in the local coordinate system of link-2. This is consistent with the third assumption that was earlier mentioned. The second requirement can be stated mathematically as follows:

$$\mathbf{g}_1^{\perp} \cdot \mathbf{g}_2 = \mathbf{0} \tag{17}$$

This reduces to the following expression:

$$R_1 R_2 \sin\left(\phi_1 - \phi_2 + \alpha\right) = 0 \tag{18}$$

The two requirements mentioned above yield three constraint equations that describe the imperfect joint. The constraint equations for the slider-crank mechanism with the simplified imperfect joint can be summarized as follows:

$$\mathbf{\Phi} = \begin{bmatrix} x_1 - l_1\cos\phi \\ y_1 - l_1\sin\phi_1 \\ -x_2 + 2l_1\cos\phi_1 + R_1\cos\left(\phi_1+\alpha\right) \\ \quad +\left[R_2 + l_2\right]\cos\phi_2 \\ -y_2 + 2l_1\sin\phi_1 + R_1\sin\left(\phi_1+\alpha\right) \\ \quad +\left[R_2 + l_2\right]\sin\phi_2 \\ R_1 R_2\sin\left(\phi_1 - \phi_2 + \alpha\right) = 0 \\ -x_3 + 2l_1\cos\phi_1 + R_1\cos\left(\phi_1+\alpha\right) \\ \quad +\left[R_2 + 2l_2\right]\cos\phi_2 \\ -y_3 + 2l_1\sin\phi_1 + R_1\sin\left(\phi_1+\alpha\right) \\ \quad +\left[R_2 + 2l_2\right]\sin\phi_2 \\ y_3 \\ \phi_3 \\ \phi_1 - \omega t \end{bmatrix} = \begin{bmatrix} 0\\0\\0\\0\\0\\0\\0\\0\\0\\0 \end{bmatrix} \tag{19}$$

Dynamic analysis can once again be done to determined the dynamic response of the system. Figure 8a. shows the reaction force for various joint clearances. As in the case of the general imperfect joint, the dynamics of the system is affected as the clearance size is changed. Also in Fig. 8b., the reaction forces for the simplified imperfect joint with zero clearance is plotted together with that of the perfect joints. The plots overlay each other confirming our expectations. Both plots were generated for the slider-crank mechanism with the parameters shown in Table 1.

Our interest in modeling the simplified imperfect joint was to incorporate the effect of wear into the dynamic analysis. Thus far we have developed an imperfect joint model for the slider-crank mechanism that can account for the changes in the system dynamics due to changes in the joint clearance. By invoking an earlier assumption, that the pin will contact the bushing at only one location, it can be shown that wear on the bushing is synonymous to increasing the clearance size. Figure 9. shows a diagram of the pin in contact with the bushing. As the pin rotates, during the motion of the mechanism, the bushing is worn out. According to the assumption, only the location where the pin first contacts the bushing is worn out. The center point of this location is shown in Fig. 9. as point *C*. It is clear from the diagram that the wear has the same effect as increasing the radius of the bushing at the center point of the contact location. Thus the wear can be simulated by simply increasing the bushing radius R_2 by an amount equivalent to the wear.

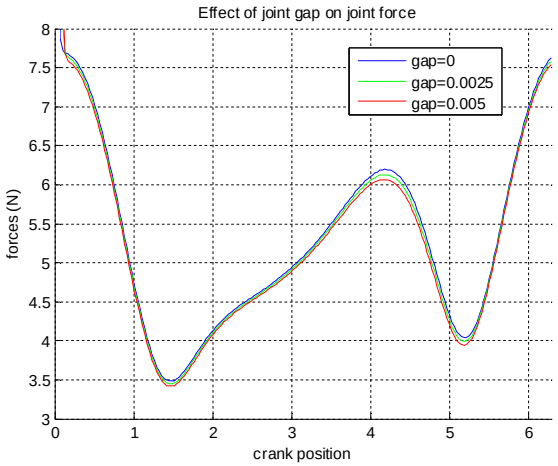

a

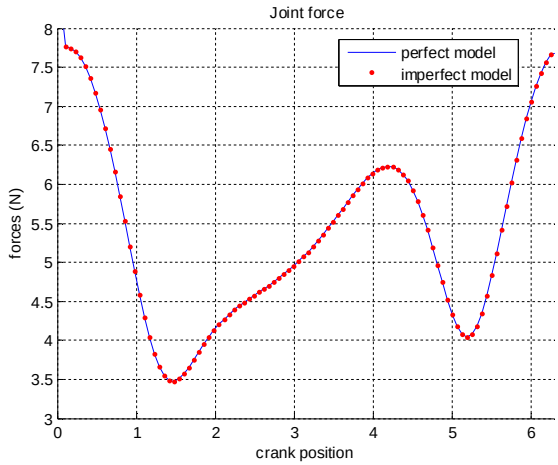

b

Figure 8: a) Reaction force for various clearance sizes (simplified joint). b) Comparison of reaction forces for the perfect and simplified joint models (zero clearance).

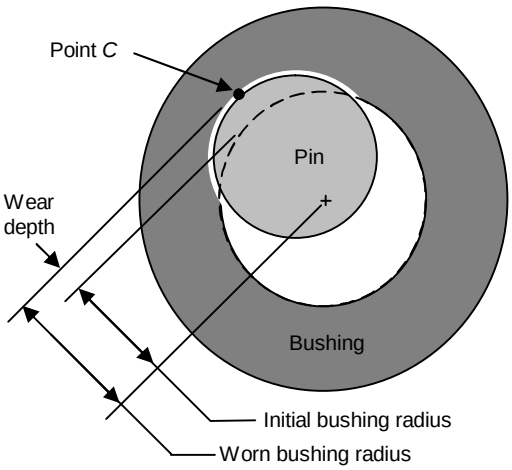

Figure 9: Wear on bushing due to the pin contact.

With both the wear prediction procedure and dynamic analysis of the slider-crank system developed, an

integrated model between the system dynamics and the wear can be created. In the following section integration of the wear analysis into the system dynamics will be discussed.

INTERGRATED MODEL: SYSTEM DYNAMICS AND WEAR PREDICTION

In order to predict the wear at the joint and also to study how the wear affects the system dynamic and vice versa, it is necessary to integrate the wear prediction procedure into the system dynamics. The integration is composed of two parts namely; dynamic analysis and wear analysis. The integration process is discussed in the following subsections.

DYNAMIC ANALYSIS - In the first part of the integration process a dynamic analysis is performed to determine the joint reaction force and the incremental sliding distance. These are the two quantities form the dynamic analysis are required to perform the wear analysis. The analysis is done for a complete cycle and the reaction force is obtained at each increment of the discretized range. The incremental sliding distance is also obtained at each increment as described by Eq. (20).

$$\Delta s_i = R_2 \bullet \left(\alpha_i - \alpha_{i-1}\right). \qquad (20)$$

In Eq. (20) α_i is the angle difference (in radians) between the local *x*- axes of the two links (see Fig. 7) at a current and α_{i-1} is the difference for a previous time. R_2 is the bushing radius. Figure 10 shows a plot of incremental sliding distance from a dynamic analysis for a slider-crank mechanism with parameters shown in Table 1. A value of 19.05mm was used for the diameter of the pin and bushing.

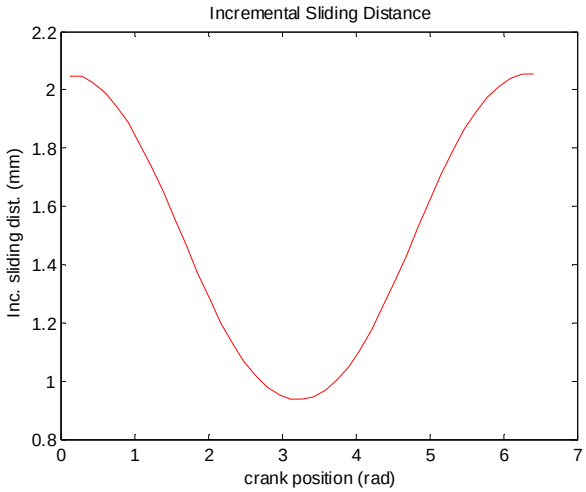

Figure 10: Incremental sliding distance.

WEAR ANALYSIS - The second part of the integration process involves a wear analysis. The amount of wear is determined at each increment based on the reaction force and sliding distance from the previous analysis and is summed (according to Eq. (5)) up to obtain the total wear for the cycle. Since the wear is equivalent to increasing the clearance, the wear amount is added to the initial joint clearance to determine the total clearance. The dynamic analysis is then repeated for the new clearance and the process is iterated up to the desired number of cycles. Figure 11 shows the flow chart for the integration process.

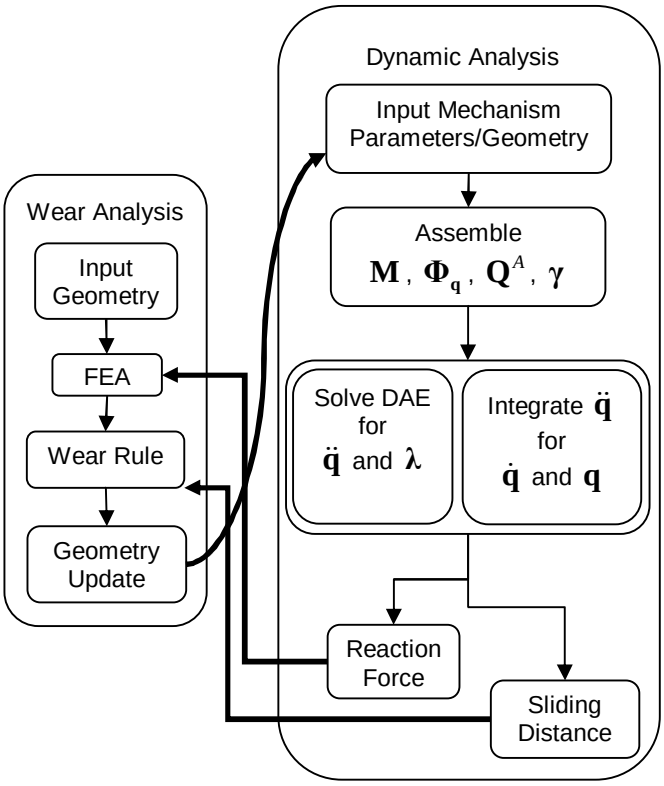

Figure 11: Integration of wear analysis into system dynamics analysis.

EXPERIMENTS FOR MODEL VALIDATION

In order to validate the integrated model an experiment was used. A diagram of the slider-crank mechanism, built for this purpose, is shown in Fig. 12. The slider-crank mechanism is built so as to minimize friction and wear (to a negligible amount) at all joints except at the joint of interest. This is achieved by building the joint between link-2 (follower) and the slider with a thrust air bearing and using a dovetail air bearing slide.

The dimensions and mass parameters for the experimental slider-crank are shown in Table 1 and Table 2. Other test parameters including the friction and wear coefficient, crank velocity, and spring constant are shown in

Table 3.

Table 3: Properties of the pin and bushing

Crank (link-1) velocity	0.5 RPM
Spring constant	525.4 N/m
Friction coefficient	0.15
Wear coefficient [25]	5.05×10^{-4} mm^3/Nm

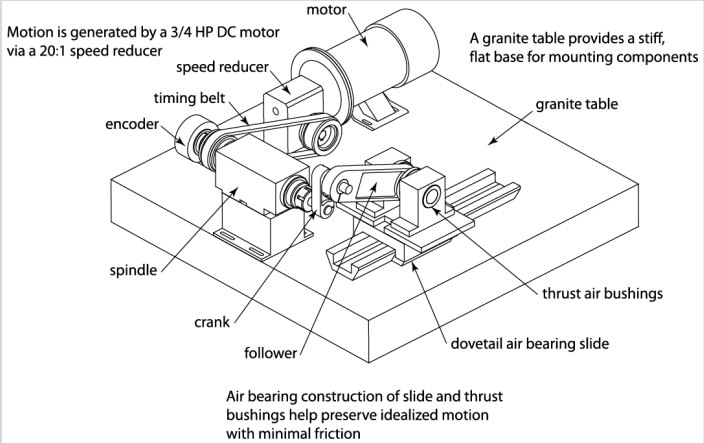

Figure 12: Experimental slider crank mechanism

The validation involves comparing the wear on the bushing, after several thousand crank cycles, obtained from the experiment and simulation tests. It was mentioned earlier that the pin is made of hardened steel so that no appreciable wear occurs on its surface. It should however be mentioned that the procedure outlined can be used to estimate the wear on both the bushing and the pin. Two sets of tests, each consisting of an experimental and simulation wear test, were conducted. In the first test a total of 32,000 crank cycles were completed while in the second test 21,400 crank cycles were completed. The simulation is conducted using the simplified imperfect joint.

Table 4 and Fig. 13 show the results from the first wear test. In Fig. 13a the initial joint reaction forces from the experiment and that from the simulation are compared. It can be seen that the simulation reaction force closely resembles that from the experiment. There is however, a discrepancy in forces at crank position of π when the slider changes direction. The discrepancy is attributed to the direction change when the slider briefly impacts the sliding rail and resulting in the higher order dynamics observed. Also in Fig. 13b, the wear profile from the experiment is shown to be reasonably predicted by the simulation model. The worn mass and maximum wear depth on the bushing are tabulated in Table 4. For both cases, the simulation reasonably predicted the experimental results.

Table 4: Wear results from test 1 (32,000 crank cycles)

	Experimental wear test	Simulation wear test	Error
Worn mass	0.2616 g	0.2336 g	10.7%
Max wear depth	0.7850 mm	0.6575 mm	16.2%
Time	17hrs	8hrs	

The results for the second set of tests are presented in Table 5 and Fig. 14. Similar to the first set of tests, the worn mass, maximum wear depth and wear profiles have been closely predicted with the simulation. It can also bee seen that the time required for the simulation is much less that would be required for the wear test, excluding the experimental set up time.

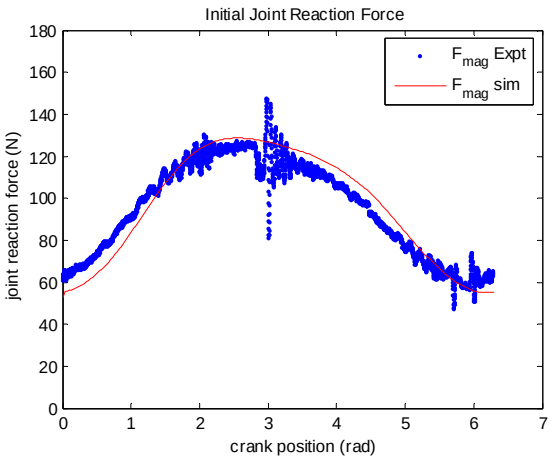

a

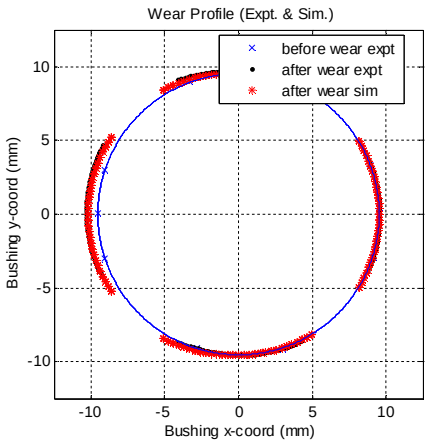

b

Figure 13: Test 1 results: 32,000 crank cycles. a) Initial joint reaction force. b) Comparison of bushing wear profile between the experiment and simulation.

Table 5: Wear results from test 2 (21,400 crank cycles)

	Experimental wear test	Simulation wear test	Error
Worn mass	0.1714 g	0.1589 g	7.2%
Max wear depth	0.4850mm	0.4524 mm	6.7%
Time	11hrs	5hrs	

One of the goals of the research was to investigate how the wear affects the dynamics and how the dynamics affects the wear. It was postulated that the system dynamics and the wear at the joints are coupled and thus evolve simultaneously. This effectively means that predicting the wear based on the initial system dynamics would lead to incorrect results. This is because the dynamics of the system changes as the wear evolves. One way to assess the coupling would thus be to

compare the wear results from the prediction based on only the initial dynamics and that based on evolving dynamics. For the current case this can be accomplished by performing a wear analysis using the slider-crank model with a perfect joint and the second model with an imperfect joint. The difference of the wear prediction will reveal the extent of the coupling.

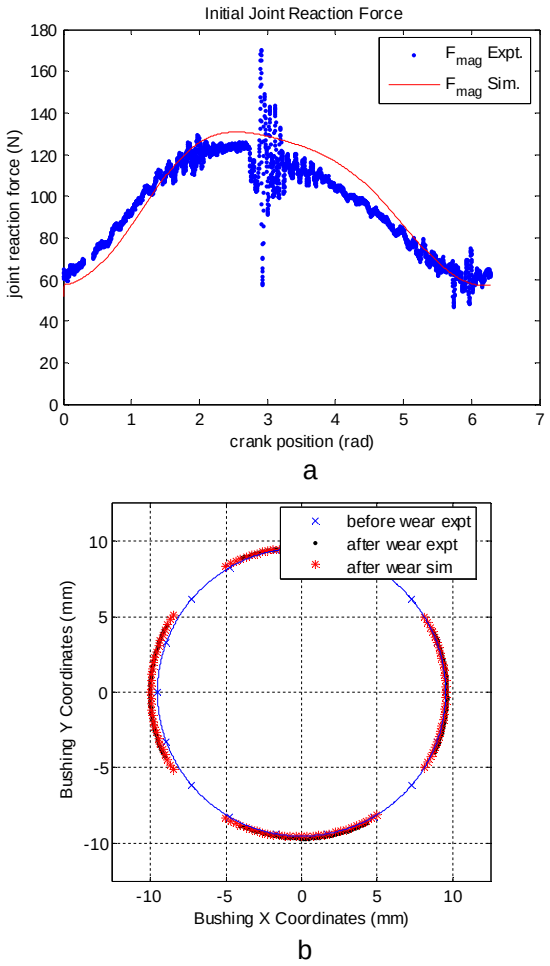

Figure 14: Test 2 results: 21,400 crank cycles. a) Initial joint reaction force. b) Comparison of bushing wear profile between the experiment and simulation.

Figure 15. shows a plot of the difference in wear prediction when only the initial dynamics is used and when evolution is system dynamics is considered. The simulation was conducted for about 95,000 crank cycles. From the plot it can be seen that as the number of cycles increases, the difference in prediction increases as well. Although the difference is small, for the current case, there is indeed some amount of coupling between the wear and the system dynamics.

DISCUSSION AND CONCLUDING REMARKS

In this work, an integrated procedure to predict the wear at a joint of a slider-crank mechanism was presented. The procedure allows for the coupling between the dynamics of the mechanism and the wear at the joint to be studied. The two main components of the procedure are the wear prediction procedure and the model of the system with imperfect joints. The wear prediction procedure discussed is an iterative procedure based on the Archard's wear law. Three models of the slider-crank mechanisms with an imperfect joint was presented. The first model represented an ideal system where no wear is experienced at the joints. The second and third slider-crank models attempted to simulate a system with an imperfect joint. In the second model, a general imperfect joint is developed where the components of the joint move relative to each other based on the dynamics of the system. Finally in the third model, a simplified imperfect joint in which the two components of the joint are in continuous contact, was developed.

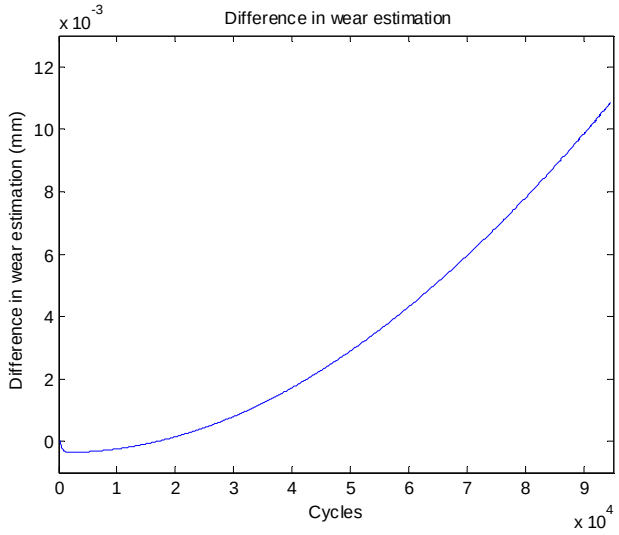

Figure 15: Difference in wear estimation between slider-crank model with perfect joints and an imperfect joint.

The integrated procedure was completed by integrating the wear prediction procedure into the dynamic analysis model. In doing so, the coupled nature of the wear at the joint and the system dynamics was studied. To validate the model, experimental wear tests were conducted. The integrated procedure was found to predict the maximum wear depth with a maximum error of approximately 16%. While this may seem large, it should be noted that there are several possible sources of error that contributed to the discrepancy. One source is in the wear prediction model which is dependent on an experimentally obtained wear coefficient and an approximation of the contact pressure (FEA). Another source of error is in the dynamic model of the slider-crank mechanism with imperfect joint. In the development of this model some assumptions were made that introduce additional errors. Nevertheless, the wear estimates are reasonably for preliminary designs.

In addition to the estimation of wear at the joint, the coupling between the wear and the dynamics of the mechanism was examined. For the mechanism, it was found that a subtle coupling exists and becomes more significant as the wear increases. The subtleness of the coupling is attributed to the simplification of the study. If further complexities were considered such as wear at other joints, flexibilities of the bodies or impact at the joints, then stronger coupling would be observed.

ACKNOWLEDGMENTS

This research was supported by National Science Foundation (DMI-0600375) and Deere & Company. Their supports are gratefully acknowledged.

REFERENCES

[1]. Dubowsky, S., 1974, "On Predicting the Dynamic Effects of Clearances in Planar Mechanisms," ASME, Journal of Eng. for Industry, pp. 317-323.

[2]. Dubowsky, S., Freudenstein, F., 1971, "Dynamic Analysis of Mechanical Systems with Clearances Part1: Formulation of Dynamic model," ASME, Journal of Engineering for Industry, pp. 305-309.

[3]. Dubowsky, S., Gardner, T.N., 1977, "Design and Analysis of Multilink Flexible Mechanisms with Multiple Clearance Connection," ASME, Journal of Engineering, pp. 88-96.

[4]. Kakizaki, T., Deck, J.F., 1993, "Modeling the Spatial Dynamics of Robotic Manipulators with Fixable Links and Joint Clearances," ASME, Journal of Mechanical Design, **115**, pp. 839-847.

[5]. Farahanchi, F., Shaw, S. W., 1994, "Chaotic and Periodic Dynamics of a Slider-Crank Mechanism with Slider Clearance," Journal of Sound and Vibration, **177**(3), pp. 307-324.

[6]. Rhee, J., Akay A., 1996, "Dynamic Response of a Revolute Joint with Clearance", Mechanisms Machine Theory, **31**(1), pp. 121-134.

[7]. Ravn, P., 1998, "A Continuous Analysis Method for Planar Multibody Systems with Joint Clearance," Multibody Systems Dynamics, Kluwer Academic Publishers, **2**, pp. 1-24.

[8]. Ravn, P., Shivaswamy, S., Alshaer, B. J., Lankarani, H. M., 2000, "Joint Clearances With Lub. Long Bearings in Multibody Mech. Systems, Journal of Mech. Design, **122**, pp. 484-488.

[9]. Ting, K.L., Zhu, J., and Watkins, D., 2000, "The Effect of Joint Clearance on Position and Orientation Deviation of Linkages and Manipulators," Mechanism and Machine Theory, **35**, pp. 391-401.

[10]. Schwab, A. L., Meijaard, J.P., Meijers, P., 2002, "A Comparison of Revolute Joint Clearance Models in the Dynamic Analysis of Rigid and Elastic Mechanical Systems," Mechanisms and Machine Theory, **37**, pp. 895-913.

[11]. Bauchau, O. A., Rodriguez, J., 2002, "Modeling of Joints with Clearance in Flexible Multibody Systems," Journal of Solids & Struct., **39**, pp 41-63.

[12]. Tsai, M.J., Lai, T.H., 2004 "Kinematic Sensitivity Analysis of Linkage with Joint Clearance Based on Transmission Quality," Mechanism and Machine Theory, **39**, pp. 1189-1206,

[13]. Flores, P., Ambro□sio, J., 2004, "Revolute Joints with Clearance in Multibody Systems," Computers and Structures, **82**, pp. 1359-1369.

[14]. Flores P., 2004, "Dynamic Analysis of Mechanical Systems with Imperfect Kinematic Joints," Ph.D. Thesis, Minho University (Portugal), Guimarães

[15]. Garcia Orden, J. C., 2005, "Analysis of Joint Clearances in Multibody Systems," Multibody System Dynamics, **13**, pp. 401-420.

[16]. Flores, P., Ambrósio, J., Claro, J. C. P., Lankarani, H. M.Koshy, C. S., 2006, "A Study on Dynamics of Mechanical Systems Including Joints with Clearance and Lubrication," Mechanism and Machine Theory, **41**, pp. 247-261.

[17]. Holm, R., 1946, *Electric Contacts*, H. Geber, Stockholm.

[18]. Podra, P. and Andersson, S., 1999, "Simulating sliding wear with finite element method," Tribology International, **32**: pp. 71-81.

[19]. Oqvist, M., 2001, "Numerical simulations of mild wear using updated geometry with different step size approaches," Wear, **249**: pp. 6-11.

[20]. McColl, I.R., Ding, J., and Leen, S.B., 2004, "Finite element simulation and experimental validation of fretting wear," Wear, **256**, pp. 1114-1127.

[21]. Hegadekatte, V., Huber, N., and Kraft, O., 2005, "Finite element based simulation of dry sliding wear," IOP Publishing, **13**, pp, 57-75.

[22]. Kim, N. H., Won, D., Buris, D., Holtkamp, B., Gessel, G. R., Swanson, P., Sawyer, W. G., 2005, "Finite Element Analysis and Validation of Metal/Metal Wear in Oscillatory Contacts," Wear, **258**, pp. 1787-1793.

[23]. Sfantos, G.K. and Aliabadi, M.H., 2006, "Wear simulation using an incremental sliding boundary element method," Wear, **260**, pp. 1119-1128.

[24]. Mukras, S., Kim, N. H., Sawyer, W. G., Jackson, D. B., and Swanson P., 2007, "Design Theory and Computational Modeling Tools for Systems with Wear", paper No. 2007-01-0892, SAE World Congress, Detroit, MI.

[25]. Schmitz L., Action, J. E., Burris, D. L., Ziegert, J. C., and Sawyer, W. G., 2004, "Wear-Rate Uncertainty Analysis", ASME, Journal of Tribology, **126,** pp.802–808.

[26]. Yang L.J., 2005, "A test methodology for determination of wear coefficient", Wear, **259**, pp. 1453–1461.

[27]. Podra, P., and Andersson, S., 1997, "Wear Simulation with the Winkler Surface Model," Wear, **207**: pp. 79-85.

[28]. Nikravesh, P.E., 1988, *Computer-Aided Analysis of Mechanical System*, Prentice-Hall, Englewood Cliffs, NJ, pp. 313-338, Chap. 13.

[29]. Haug, E. R., 1989, *Computer-Aided Kinematics and Dynamics of Mechanical Systems*, Allyn and Bacon, Needham Heights, US-MA, pp. 248-259.

[30]. Hamid, M.L., Parviz, E.N., 1994, "Continuous Contact Force Model for Impact Analysis in Multibody Systems", Nonlinear Dynamics, Kluwer Academic Publishers, **5**, pp. 193-207.